JTTEE5 14:373-383
DOI: 10.1361/105996305X59369
1059-9630/$19.00 © ASM International

Effects of Spray Conditions on Coating Formation by the Kinetic Spray Process

Taeyoung Han, Zhibo Zhao, Bryan A. Gillispie, and John R. Smith

(Submitted September 2, 2004; in revised form November 17, 2004)

The kinetic spray coating process involves impingement of a substrate by particles of various material types at high velocities. In the process, particles are injected into a supersonic gas stream and accelerated to high velocities. A coating forms when the particles become plastically deformed and bond to the substrate and to one another upon collision with the substrate. Coating formation by the kinetic spray process can be affected by a number of process parameters. In the current study, several spray variables were investigated through computational modeling and experiments. The examined variables include the temperature and pressure of the primary gas, the cross-sectional area of the nozzle throat, the nozzle standoff distance from a substrate, and the surface condition of nozzle interior and the powder gas flow. Experimental verification on the effects of these variables was performed primarily using relatively large-size aluminum particles (63-90 μm) as the feedstock material. It was observed that the coating formation is largely controlled by two fundamental variables of the sprayed particles: particle velocity and particle temperature. The effects of different spray conditions on coating formation by the kinetic spray process can be generally interpreted through their influences on particle velocity and/or particle temperature. Though it is limited to accelerate large particles to high velocities using compressed air or nitrogen as carrier gas, increasing particle temperature provides an additional means that can effectively enhance coating formation by the kinetic spray process.

Keywords coating formation, computational fluid dynamics, deposition efficiency, discrete particle simulations, kinetic spray process, metallic powders, spray parameters

1. Introduction

The kinetic spray process is a relatively new process that involves using high velocity particles to generate surface coatings (Ref 1-11). A kinetic spray nozzle system is schematically shown in Fig. 1. In this process, powder particles are injected into a supersonic gas stream and accelerated to high velocities. When the particles impinge upon a substrate, the powder particles deform plastically and bond to the substrate and one another to form a coating. In general, the inlet gas flow is heated to elevated temperatures to accelerate the particles to higher velocities. However, the temperatures of both the gas flow and the particles are well below the melting temperature of the coating material. Thus the kinetic spray process is a relatively low-temperature process compared with conventional thermal spray processes. The kinetically sprayed coatings are often characterized by relatively little oxidation, low residual stresses, high deposition rates, and good coating-substrate bonding (Ref 3-9). With the relatively low process temperatures, the kinetic spray process does not cause phase transformations and composition variations that may otherwise occur in the spray processes involving high temperatures or melting, making this coating process particularly useful for thermally sensitive materials.

In the kinetic spray process, the velocity of the sprayed powder particles is considered as a key physical quantity that critically affects the coating formation. For a given powder-substrate combination, a critical velocity of powder particles was suggested, above which coating formation occurs (Ref 3-5). Therefore, the ability to manipulate spray conditions of the kinetic spray process to maximize particle velocities is highly desirable to enhance the coating formation by the kinetic spray process. This is particularly true if one wants to use nitrogen or compressed air (instead of helium) as carrier gas and large size particles as feedstock. Because the kinetic spray process is a relatively new coating process, the effects of spray variables on coating formation have been conducted to much lower degrees, compared with various thermal spray processes. In the previous studies, various spray parameters were investigated in terms of its effect on particle velocities (Ref 5, 8, 11). This work presents a systematic study including additional important kinetic spray parameters, in an attempt to provide some guidance to improve the coating formation.

Computational modeling of the kinetic spray process was performed along with experimental studies to understand the complex interactions between the gas flow and particle dynamics. The Navier-Stokes equations are solved for the gas flow with a discrete particle model to track the particles injected in the gas flow. In addition to the temperature and pressure of the main gas, the effects of other less prominent variables on the kinetic spray process were also examined. These include the size of the nozzle throat, surface condition of nozzle interior, standoff distance, and powder gas flow rate. Furthermore, it is recognized in the current study that sprayed particles can be softened at elevated temperatures and thus plastically deformed more easily in the kinetic spray process. In other words, the increased particle temperature can effectively lower the critical particle velocity, thus enhancing the coating formation.

Accordingly, particle temperature is treated as a fundamental variable in addition to particle velocity in the kinetic spray process. To simulate particle velocity and particle temperature, the

Taeyoung Han, Zhibo Zhao, Bryan A. Gillispie, and **John R. Smith,** Delphi Research Labs, 51786 Shelby Parkway, Shelby Township, Michigan 48315. Contact e-mail: taeyoung.han@delphi.com.

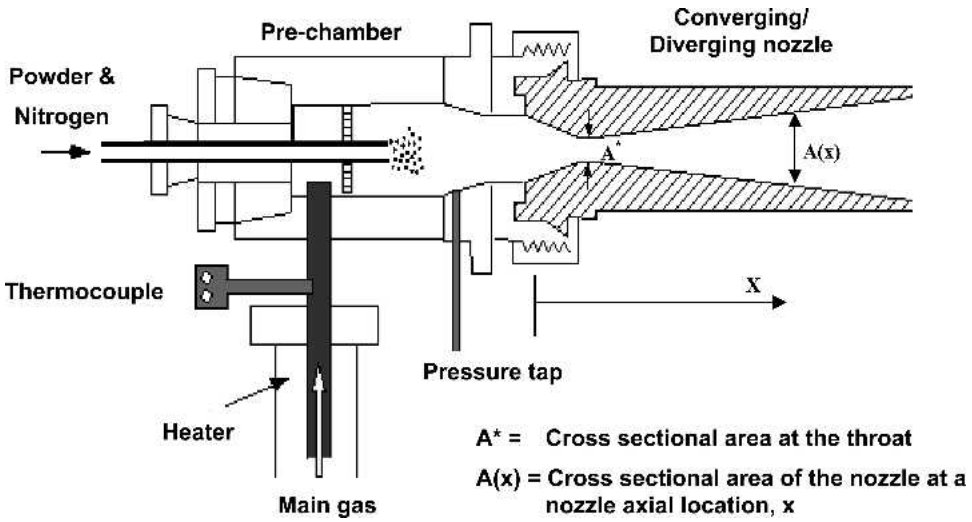

Fig. 1 Schematic illustration of the kinetic spray nozzle configuration

computational model and the basic gas dynamics for the kinetic spray process are outlined in section 2. The experimental procedures for coating deposition via the kinetic spray process are described in section 3. In Sec. 4, we present modeling and experimental results, along with the discussions on the effects of spray conditions on the coating formation. Then, the major findings of this work will be summarized in section 5.

2. Basic Gas Dynamics and Computational Model

To explain basic compressible gas dynamics in a nozzle, a one-dimensional isentropic flow is first considered. Assuming the flow is adiabatic and frictionless, one can calculate the state values of the gas pressure P, temperature T, and velocity u, throughout the nozzle. The changes of these gas state values are simply dependent on the local Mach number M and the gas specific heat ratio γ. The local Mach number is defined as:

$$M = \frac{u}{c} \qquad \text{where } c = \sqrt{\gamma \mathrm{R} T} \tag{Eq 1}$$

R is the gas constant, and c is the speed of sound. The Mach number M can be derived as a function of the local area ratio A/A^* and the gas specific heat ratio γ (Ref 12):

$$\frac{A}{A^*} = \frac{1}{M}\left[\left(\frac{2}{\gamma+1}\right)\left(1+\frac{\gamma-1}{2}M^2\right)\right]^{(\gamma+1)/2(\gamma-1)} \tag{Eq 2}$$

where A is the local cross sectional area of the nozzle and A^* is the nozzle throat area.

The total mass flow rate through the nozzle is:

$$\dot{m} = \frac{P_\mathrm{o}}{\sqrt{T_\mathrm{o}}} A^* \sqrt{\frac{\gamma}{\mathrm{R}}}\left(\frac{\gamma+1}{2}\right)^{-(\gamma+1)/2(\gamma-1)} \tag{Eq 3}$$

For a given operating inlet condition, from Eq 3, the total mass flow rate through the converging-diverging nozzle increaseslinearly with the total inlet pressure P_o and the throat area A^*. However, the mass flow rate decreases with square root of the inlet gas temperature T_o.

Once the gas flow field becomes known in a nozzle, the particle acceleration and the heat transfer to the particles can be calculated. The acceleration of a particle due to the drag force D is expressed by:

$$m_\mathrm{p}\frac{dU_\mathrm{p}}{dt} = \frac{1}{2} C_\mathrm{D}\rho(u-U_\mathrm{p})^2 A_\mathrm{p} \tag{Eq 4}$$

where u and U_p are the gas and particle velocities, ρ is the gas density, m_p is the particle mass, A_p is the projected cross-sectional area of the particle perpendicular to the flow, and C_D is the drag coefficient of the particle. Note that C_D is a function of the Reynolds number and the Mach number (Ref 13). For a given drag force on a particle, the trajectory and the velocity of a particle can be obtained from Eq 4.

In considering particle temperatures, one has to examine the Biot number for metallic particles in a heated gas flow. The Biot number can be represented by $Bi = hd/k_\mathrm{p}$, where h is the convective heat transfer coefficient, d the particle diameter, and k_p the heat conductivity of the spray material. Due to the relatively high heat conduction within the metallic particles, the Biot number for the kinetic spray application is typically less than 0.1. Thus, it is reasonable to assume the particle temperatures as homogeneous within individual particles. Then the heat transfer between gas and particle can be modeled from the following equation:

$$m_\mathrm{p} Cp_\mathrm{p}\frac{dT_\mathrm{p}}{dt} = S_\mathrm{A} h(T_\mathrm{r} - T_\mathrm{p}) \tag{Eq 5}$$

where Cp_p is the particle specific heat, T_p the particle temperature, and S_A the surface area of the particle. T_r is the so-called recovery temperature, namely the gas temperature in the boundary layer, which may be much higher than the free stream gas temperature due to viscous heat dissipation. The convective heat

transfer coefficient h can be obtained from the following Nusselt number correlation applicable for high Mach numbers (Ref 14):

$$Nu \equiv \frac{hd}{k_g} = \frac{2 + 0.459Re^{0.55}Pr^{0.33}}{1 + \frac{3.42M(2 + 0.459Re^{0.55}Pr^{0.33})}{RePr}} \quad \text{(Eq 6)}$$

where Pr is the Prandtl number, Re the Reynolds number, and M the Mach number. The gas thermal conductivity k_g should be evaluated at T_r, the recovery temperature.

The one-dimensional isentropic flow analysis is useful in gaining a basic understanding of ideal gas flow in the nozzle. However, it cannot represent a real three-dimensional (3D) gas flow that includes wall friction and turbulent mixing between the heated main gas and the low-temperature powder gas flows. To capture more realistic features of kinetic spray process including the effects of gas and particle interactions and turbulent mixing, computational simulations were conducted in connection with experimental studies. Applying computational fluid dynamics (CFD), one can predict the gas flow characteristics inside the converging/diverging nozzle and the impinging supersonic turbulent jet on the substrate. The governing equations are the mass, momentum, and energy conservation equations for both gas flow and particle dynamics.

The CFD code FLUENT is capable of treating interactions between the gas phase and the powder particles in terms of momentum and energy (Ref 15). Previously, FLUENT simulation was applied to optimize the cold-spray process (Ref 16). In the current study, a standard k-ε turbulence model is used to account for turbulence in the flow (Ref 17). As the gas flow is compressible, the density variations in the field are predicted based on the ideal gas law. For boundary conditions, the operating pressure and the temperature are specified for the primary gas where the flow is subsonic. At the location where the particles are injected into the gas stream, one specifies the powder gas flow rate, the powder feed rate, and the particle size. At the nozzle walls, the nonslip condition is used with the turbulent wall function (Ref 17).

Depending on powder feed rate, the main gas flow can influence discrete particles and vice versa. Therefore, the interaction of particles with the gas flow was taken into consideration in the simulations. In a coupled approach, calculations of the gas flow phase and the discrete particle phase were alternated until a converged coupled solution is achieved. Using the code FLUENT, the particle trajectories are computed both in the nozzle and in the downstream of the nozzle exit until the particles collide with a substrate. The dispersion of particles due to turbulence in the gas flow can also be considered via the stochastic tracking model (Ref 18). Such a model includes the effect of instantaneous turbulent velocity fluctuations on the particle trajectories. The details of these physical models for discrete particle interactions with turbulent flows are described in Ref 15. A typical 3D mesh is shown in Fig. 2. The total number of finite volumes is about 20,000 cells for an axial-symmetric model and about a half million cells for a 3D model to obtain accurate numerical solutions. To check the numerical accuracy of the computational model, the 3D computational model was simulated under inviscid and adiabatic flow assumption for comparison with the theoretical isentropic flow solution. This is a useful procedure to investigate

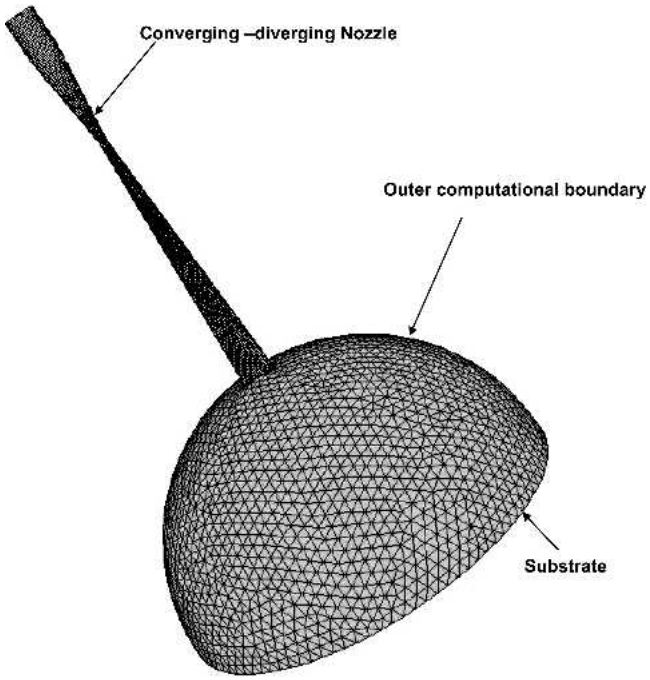

Fig. 2 Computational domain and the 3D mesh on the computational domain; mesh types are a combination of hex and tetra elements

the effects of "numerical diffusion (or false diffusion)" on the accuracy of CFD solutions. The numerical diffusion could be introduced when the convection terms in the Navier-Stokes equations are approximated by various discretization schemes. In this work, the 3D computational simulation with the inviscid and adiabatic flow assumption predicted fairly well the gas flow Mach numbers, pressures, and temperatures in the nozzle compared with the theoretical 1D isentropic flow solutions. For example, Fig. 3 shows the computed Mach numbers and a direct comparison with the theoretical solution (Ref 12), indicating a good agreement between the two results. The 3D simulation result also shows that the Mach numbers decrease rapidly due to a compression shock at the nozzle exit and becomes zero at the substrate. To understand the effects of the gas viscosity on the pressure drop, inviscid flow case was compared with the laminar flow and turbulent flow cases shown in Fig. 4. For both laminar and turbulent flow cases, there was no shock formation in the nozzle. Strong interactions of the supersonic jet with the free stream occur right after the nozzle exit due to very high shear rate around the supersonic jet. As shown in Fig. 4, the effect of the gas viscosity on the gas pressure appears relatively insignificant for rapidly accelerating flows.

3. Experimental Procedures

The kinetic spray facility at Delphi Research Laboratories was used for the experimental studies of coating deposition. A detailed description of the kinetic spray process and the facility was reported previously (Ref 8, 9). Two types of spray nozzles were used in the current study. They are nearly identical in terms of shape, geometry, and dimensions except for the sizes of their

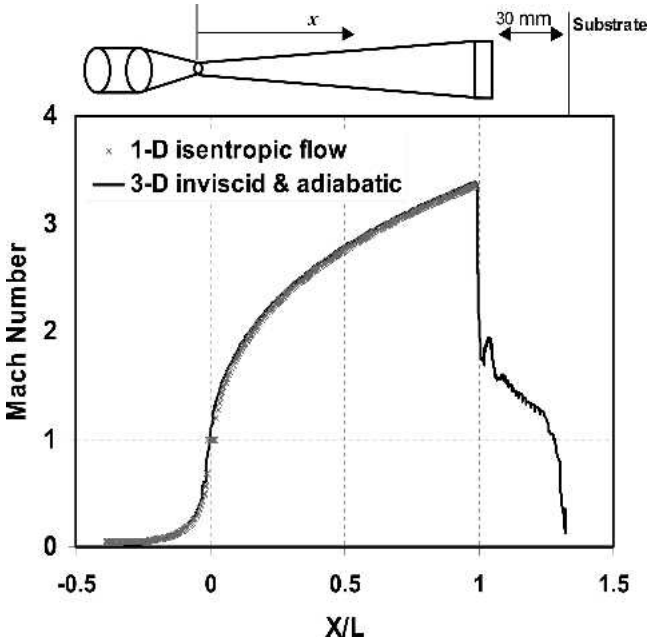

Fig. 3 3D inviscid flow simulations to compare with an isentropic flow case for Mach numbers in a converging diverging nozzle with 2 mm throat

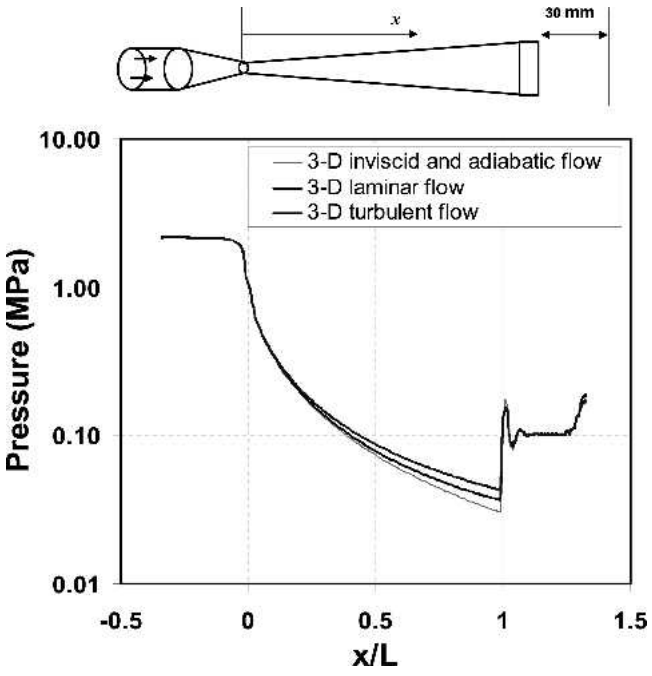

Fig. 4 Pressure distribution in the converging and diverging nozzle for three different flow assumptions; inviscid, laminar, and turbulent flows

throats and exits: one has a 2 mm diameter throat with 2 × 10 mm exit, and the other has a 2.83 mm diameter throat with 4 × 10 mm exit. The exit of the nozzle is a rectangular shape and the nozzle expansion ratios for these two nozzles are the same as 6.37. Although a circular exit nozzle is desirable for the gas flows, the rectangular exit shapes were chosen to maximize the coverage of

Fig. 5 Morphologies of the gas atomized aluminum powder particles

the coating surface areas. The total length of the nozzle is 121 mm, and the length between the throat and the exit is 88 mm. The aluminum powder, supplied by Valimet, was prepared using a gas atomization process. The particle size distribution of the powders was 63-90 μm and their morphologies are shown in Fig. 5. The feedstock powders were injected into the spray nozzle using a high-pressure powder feeding system with calibrated powder feed rate. Both the powder feed gas and the main gas were compressed nitrogen. Al alloy strips, mounted on a computer-controlled XYZ stage, were used as substrates. During coating deposition, the substrates were translated at controlled traverse speeds in front of the spray nozzle. This led to coatings with varying mass loadings (defined as weight gain per unit area). The powder particles are fed with a high-pressure powder feeder, and the powder feed rate was kept at 1 g/s in the current study. The loading of a deposited coating was determined by measuring the weight of the sample before and after deposition, and deposition efficiencies of the coatings were calculated based on their mass loadings and consumed powder particles.

4. Results and Discussion

In the following sections, the effects of various spray variables on coating deposition are discussed in terms of loading behavior, deposition rate, and deposition efficiency of the coatings.

4.1 Effect of Inlet Gas Temperature and Pressure

One-dimensional isentropic flow simulations, based on Eq 2, 4, and 5, were performed to understand the effects of operating gas pressures and temperatures on particle velocities and temperatures. The nozzle throat is assumed to be 2.83 mm, with the nozzle expansion ratio of $A/A^* = 6.37$. Figures 6 and 7 show the computed results of the velocity and the temperature of aluminum particles (63 μm diameter) at the nozzle exit. Generally speaking, the particle velocity can be increased by raising either the inlet gas pressure or the gas temperature. Such a result is not unexpected and was also indicated in the previous studies (5,

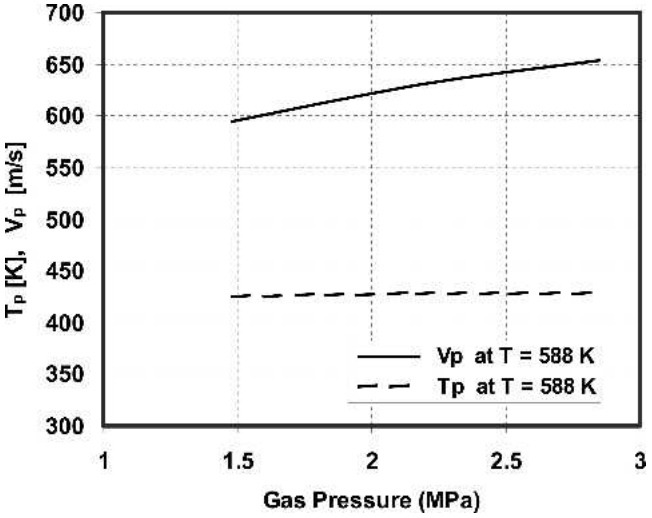

Fig. 6 Effects of main gas pressure on particle velocity and temperature (assume 63 μm Al particle) at a gas temperature of 588 K

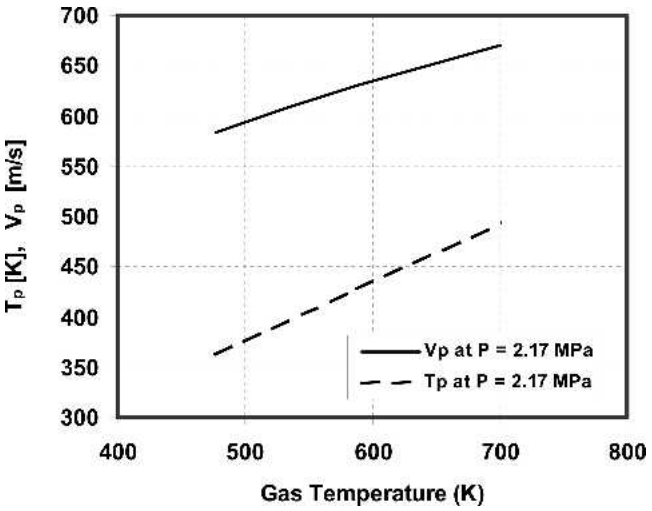

Fig. 7 Effects of main gas temperature on particle velocity and temperature (assume 63 μm Al particle) at a gas pressure of 2.17 MPa

11). However, it is of particular interest to note the effects of the inlet gas condition on the particle temperature. Smaller variations are shown as a function of gas pressure, and the particle temperature exhibits strong dependence on the gas temperature. As shown in Fig. 7, the temperature of a 63 μm Al particle can reach as high as 500 K at the inlet temperature of 700 K. Around particle temperature of 500 K, certain types of metallic particles can be significantly softened, promoting plastic deformation during coating formation by the kinetic spray process. For example, the yield strength of Al decreases from 130 MPa at room temperature to 40 MPa at approximately 500 K. Figure 8 shows experimental data of the deposition efficiencies of aluminum powder particle (63-90 μm) deposited at different inlet gas temperatures. Other spray conditions were kept the same in the test: the powder feed rate of 1 g/s, the inlet gas pressure was of 2.07 MPa (300 psi, gauge pressure), and the powder gas pressure of

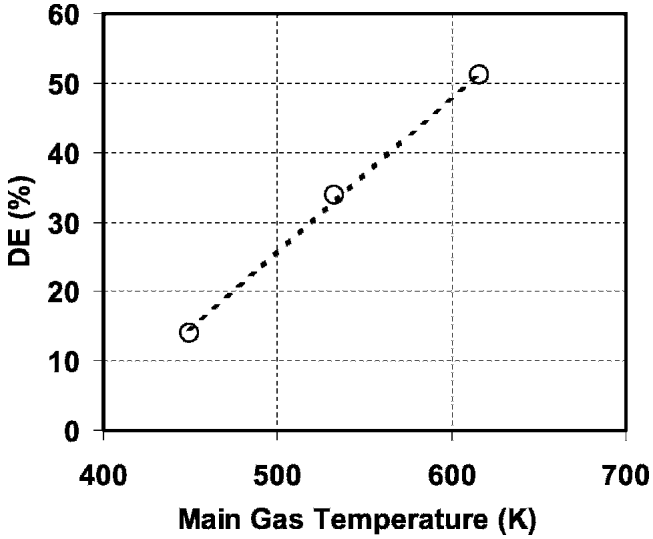

Fig. 8 Effects of the main gas temperature on the deposition efficiency of aluminum powders (63-90 μm) at a traverse speed of 2.5 cm/s

2.41 MPa (350 psi, gauge pressure). The result for the relatively large aluminum particles indicates that the deposition efficiency increases linearly with increasing the inlet gas temperature. This can be attributed to both increased particle velocity and enhanced particle temperature. Though particle temperature may not play a significant role when relatively low temperature helium is used for small particles (Ref 5, 11), it could become a significant variable when using compressed nitrogen as propellant gas for relatively large particles. In this case, much higher gas temperatures (up to ~1000 K) are required to achieve reasonably high deposition efficiency for large size particles. Accordingly, this offers the possibility for metallic particles to be heated to elevated temperatures at which materials may be significantly softened for ease in coating formation by the kinetic spray process.

4.2 Effect of the Nozzle Throat Area

From Eq 3, the throat area of the spray nozzle is a primary factor governing the mass flow rate of the main gas. For a given inlet condition, the total mass flow rate through a converging-diverging nozzle is linearly proportional to the throat area when the gas flow is choked at the throat section. When such a condition occurs, the nozzle is passing the maximum possible mass flow rate. Under free flow conditions (i.e., without injecting powder feed gas), the measured flow rate of the nitrogen at temperature of 643 K and pressure of 2.07 MPa is roughly 1.04 m^3/min for a 2.83 mm (throat diameter) nozzle and 0.56 m^3/min for a 2.0 mm (throat diameter) nozzle. From one-dimensional isentropic flow analysis, the same gas velocities at the nozzle exits are expected due to the same expansion ratios of these two nozzles. However, this is true only for the case of a very low powder feed rate, where the momentum of the main gas flow is not affected by the particles. In the case of relatively high powder feed rates, the main gas flow is disturbed by particle interactions. The overall capacity of the nozzle for a large powder feed rate depends on the total kinetic energy of the gas flow. The

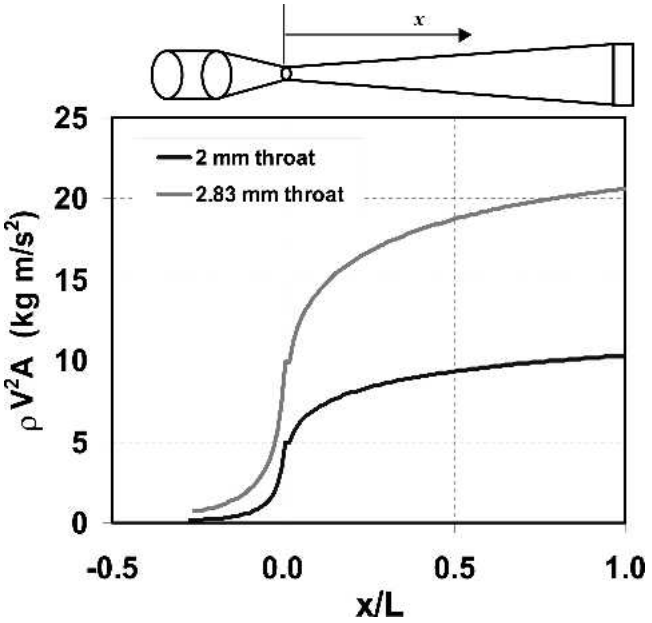

Fig. 9 Variation of the kinetic energy of the carrier gas multiplied by local cross-sectional areas for two nozzles with different throat diameters and the same exit area

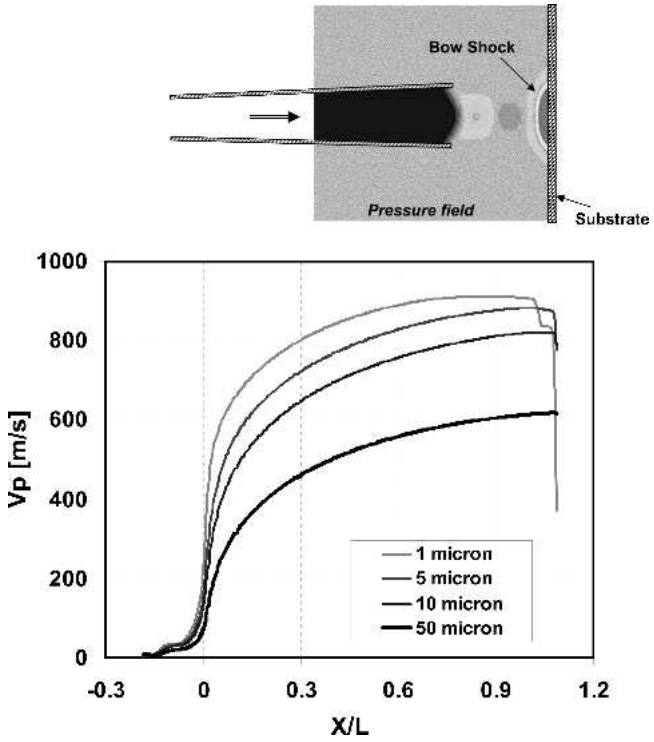

Fig. 10 Effects of bow shock on the particle velocities for various aluminum particle sizes

overall particle acceleration potential from the gas flow is proportional to $\rho V^2 A$, where ρ and V are the density and velocity, respectively, of the gas in the nozzle and A is the local flow area of the nozzle. In other words, the particle acceleration potential is the product of the mass flow rate (ρVA) and the gas velocity (V). Figure 9 shows the variation of the total kinetic energy along the nozzle axis for the two nozzles with different throat areas (but same nozzle exit area). The result suggests that the nozzle with the 2.83 mm throat diameter produced a much higher kinetic energy throughout the nozzle. Our experiments showed that the 2.0 mm throat diameter nozzle was limited to primarily the relatively soft metallic particles (63-90 μm) such as Al, Cu, and Zn. However, when used to spray relatively hard alloy powder particles such as the eutectic Al-Si alloy (63-90 μm, the Vickers's hardness is about six times of Al), the nozzle with the 2.0 mm throat diameter consistently performed poorly, compared with the one with the 2.83 mm throat diameter. In practice, it is often limited for a single spray variable to be adjusted to enhance coating formations. Therefore, the effect of throat size as observed here suggests that an increase in the mass flow rate provides an additional leverage when other variables (for example the main gas temperature) reach their limits when dealing with difficult to deposit materials.

4.3 Effects of the Standoff Distance

Depending on the spray standoff distance, a bow shock wave occurs near the substrate where the impinging supersonic jet decelerates rapidly in front of the substrate. There are abrupt changes in the flow properties, such as pressure, temperature, density, and velocity across the bow shock. The bow shock wave decelerates the gas flow to a subsonic velocity. Across the bow shock, the particles could be slowed down due to increased gas density and decreased gas velocity. In particular, small aluminum particles are easily decelerated by the compression shocks and are severely deflected before they reach the substrate, as shown in Fig. 10. However, the large aluminum particles (>50 μm) appear to be able to penetrate the compression shock near the substrate with little deceleration. Apparently, this is due to the relatively large inertia of these particles. Smaller aluminum particles, less than 10 μm diameter, show considerable deceleration in the compression shock. Based on the computational analysis, the formation of the compression shock wave in front of the substrate appears to be of little significance in the case of spraying relatively large particles within the examined standoff distance between 10 and 30 mm. In general, the strength of the compression shock decreases with the further increase of the standoff distance. However, large standoff distances may lead to turbulent jet instabilities, which could adversely affect coating formation (Ref 19).

The effect of standoff distance on coating deposition by the kinetic spray process was examined experimentally. Figure 11 shows the deposition efficiencies of aluminum powder particles (63-90 μm) with varying standoff distance. The variations of deposition efficiency have slight tendency to decrease with the stand-off-distance due to a lower substrate temperature with the large stand-off-distance, which is due to reduced aerodynamic wall friction at the substrate. However, the variations are relatively insignificant when the stand-off-distance is varied from 10 to 30 mm. This result, along with the previous work on spraying other type of materials, suggests that standoff distance (within the range examined in the current study) has relatively minor effect on coating deposition by large particles. As a result

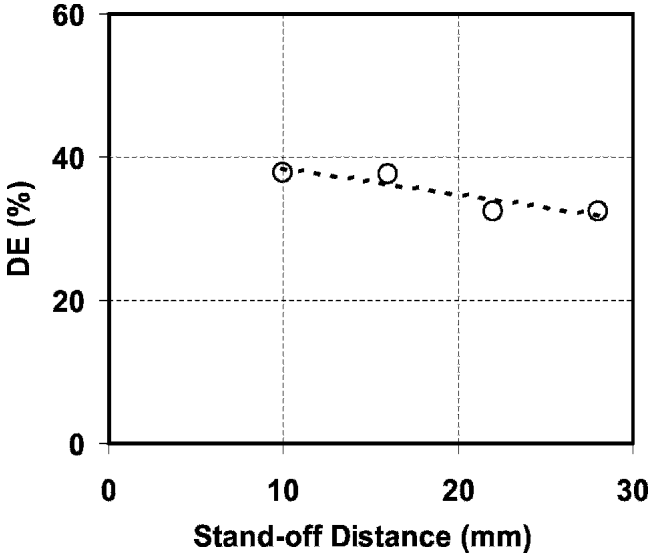

Fig. 11 Effects of standoff distance on the spraying of aluminum coatings. The standoff distance is the distance between the substrate and the exit of the spray nozzle.

of this observation, a fixed standoff distance (20 mm), unless specified otherwise, was used for the spray experiments in the current study.

4.4 Effects of Surface Condition of the Nozzle Interior

The conditions of the nozzle interior surface can have a strong effect on coating formation by the kinetic spray process. This is especially true when the deposited materials have a high tendency to build up onto the nozzle interior surface. Powder particles of ductile metals/alloys tend to become softer and "gummy" when they are heated up by the carrier gas. As a result, certain particles are likely to build up onto the heated nozzle interior surface when the inlet gas temperature is sufficiently high. Such a buildup, even without reaching the point that drastically reduces the gas flow, could have a profound effect on coating deposition. One example is shown in Fig. 12, which compares the coating depositions by a clean nozzle and a nozzle with particle buildup. In some cases, such a build-up layer is extremely thin and can easily be overlooked without scrutiny. To understand its effect on coating deposition, one may consider such a build-up layer as an added roughness to the interior surface of a spray nozzle. Then the roughened surface causes turbulence and thickens the boundary layers adjacent to the interior wall surfaces. Consequently, fewer powder particles achieve critical velocities for coating formation to occur. The effects of wall roughness on the gas flow can be simulated through the "law-of-the-wall" model for turbulent flows (Ref 17). The law-of-the-wall is a semiempirical wall function that links the velocity at the near wall cells and the roughness on the wall. The general form of the wall function can be written as:

$$\frac{u_p u^*}{\tau_w/\rho} = \frac{1}{\kappa}\ln\left(E\frac{\rho u^* y_p}{\mu}\right) - \Delta B \qquad \text{(Eq 7)}$$

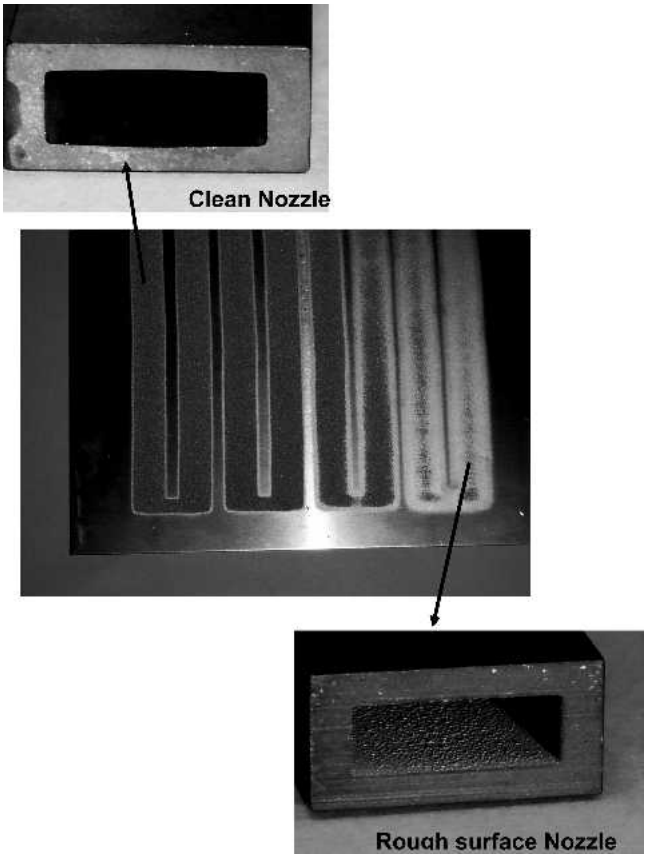

Fig. 12 Test results showing the degradation process of coating formation, as metal powders with a low melting temperature (such as Al) tend to build up on the nozzle interior surface

where κ is the von Karman constant (= 0.42), E is the Empirical constant (= 9.81), u_p is the mean fluid velocity near the wall, y_p is the distance from the wall, μ is dynamic viscosity of the fluid, $u^* = C_\mu k^{1/2}$, C_μ is the turbulent flow empirical constant, k is the turbulent kinetic energy, τ_w = wall shear stress, and ΔB is a roughness function that quantifies the effects of wall roughness. ΔB depends on the type and size of the roughness and has been found to be well correlated with the nondimensional roughness height K_S^+:

$$K_S^+ = \frac{\rho K_S u^*}{\mu} \qquad \text{(Eq 8)}$$

where K_S is the physical roughness height. It was indicated in Ref 20 and 21 that generally the roughness function is not a single function of K_S^+, and for a fully rough regime ($K_S^+ > 90$), the roughness function becomes:

$$\Delta B = \frac{1}{\kappa}\ln(1 + C_k K_S^+) \qquad \text{(Eq 9)}$$

where C_k, the roughness constant, is a measure of uniformity of the roughness and is dictated by the type of the roughness. In the present simulations of wall roughness, we considered a range of

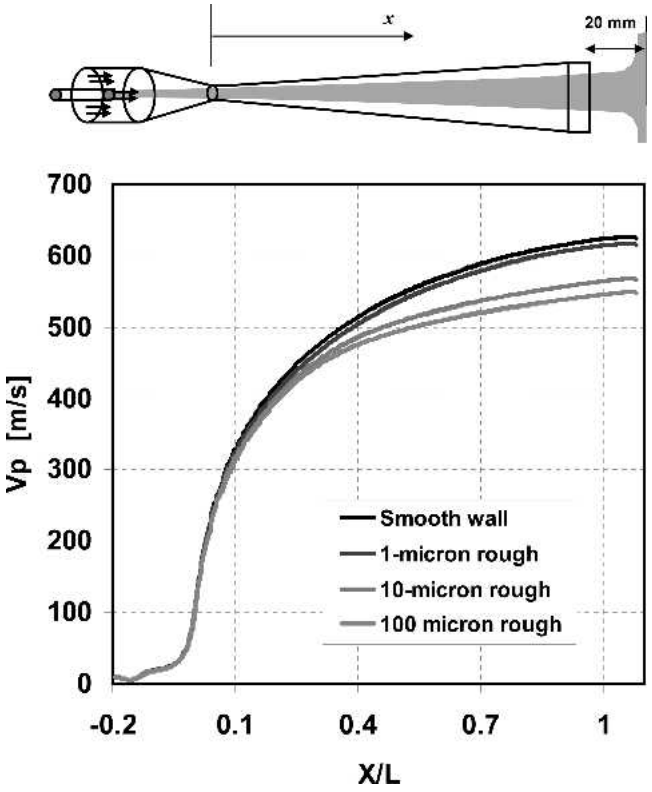

Fig. 13 Effects of interior nozzle surface roughness on aluminum particle velocity

wall roughness conditions (smooth wall, 1, 10, and 100 μm wall roughness) to examine the effect of wall roughness on particle velocities. Figure 13 shows the centerline velocity distribution along the nozzle for a 63 μm aluminum particle under different wall roughness conditions. While 1 μm wall roughness shows little effect on the particle velocity, there is significant reduction in the particle velocities for 10 and 100 μm wall roughnesses. The actual roughness in the nozzle caused by particle accumulation can be estimated to be approximately between 10 and 100 μm for sprayed particles with size between 63 and 90 μm. With such a range of surface roughness, the CFD simulations predict a reduction in particle velocity by roughly 70-80 m/s at the point of impact on the substrate. Therefore, the particle velocity becomes lower than the critical velocity. This explains the degradations in coating deposition by the particle buildup at nozzle interior surface, as manifested by the experimental observation shown in Fig. 12.

4.5 Effects of Powder Gas Flow Rate

As shown in Fig. 1, the powder particles are injected through a powder injector (a small stainless steel tube) into the prenozzle chamber, where the powder intermixes with the heated main gas. The powder gas flow that carries the powder particle from the powder feeder to the injector is at room temperature. The powder gas flow is controlled primarily by the size of the injector and the differential pressure between the powder feeder and the prenozzle chamber. Because the injector is largely submerged

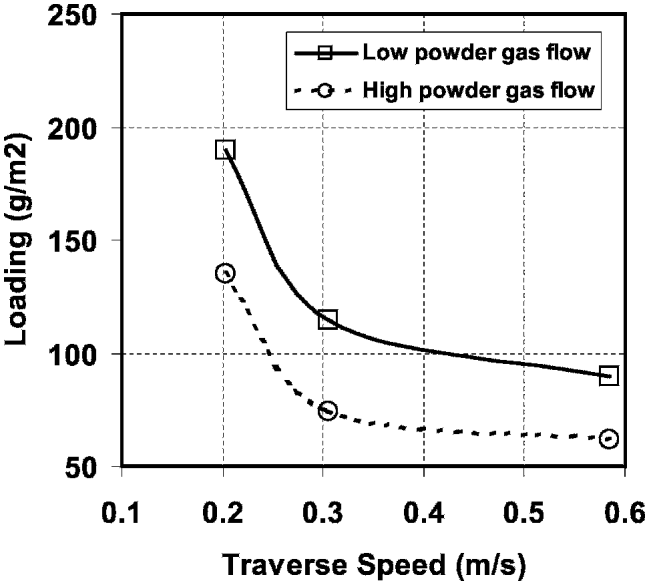

Fig. 14 Effect of the powder gas flow rate on the deposition per unit area for Al coatings

inside the heated gas flow, a sufficient powder gas flow is needed to prevent the injector from buildup/clogging by particles. However, it was also observed that too much powder gas flow can degrade coating formation. Figure 14 shows the effects of powder gas flow on Al coatings deposited using 63-90 μm particles. Note that under the same nominal spray conditions, spraying with the smaller nitrogen flow rate (2.8 g/s) consistently resulted in coatings with higher deposition than with the larger powder gas flow rate (6.1 g/s). This phenomenon can be explained from the following computational simulations.

The carrier gas is actually a mixture of the heated main gas (nitrogen) and the room-temperature powder feed gas (nitrogen). Only the main gas is heated to elevated temperatures, and the powder feed gas is at a room temperature. To observe mixing of high and low temperature gas flows and the gas temperature distribution in the nozzle before the throat section, simulations using FLUENT were performed for an axially symmetric nozzle with a throat diameter of 2.8 mm with the nozzle expansion ratio of 6.34. Figure 15 shows the temperature distributions for the two cases of different powder gas flow rates: of 6.1 g/s (= 5.3 l/s) and 2.8 g/s (= 2.5 l/s). The total mass flow rate through the nozzle can be determined by Eq 3 when the gas flow is choked at the throat section. For the operating conditions given in Fig. 15, the total gas mass flow rate was computed as 20 g/s (= 17.5 l/s), which is consistent with the experimental value. In other words, the main gas flow rate varies with the powder gas flow rate to maintain a nearly constant total inlet gas flow. As shown in Fig. 15, the average temperatures of the mixed gas at the throat section are 580 and 635 K, respectively, for the higher and lower powder gas flow rates. Furthermore, the particle velocity, particle residence time within the heated gas stream and particle temperature were also calculated, and the results are shown in Fig. 16, 17, and 18, respectively. With the lower powder gas flow rate, the particle velocity (particles with a 63 μm diameter) was predicted smaller as compared with the high powder gas flow rate in the converging section of the nozzle before the

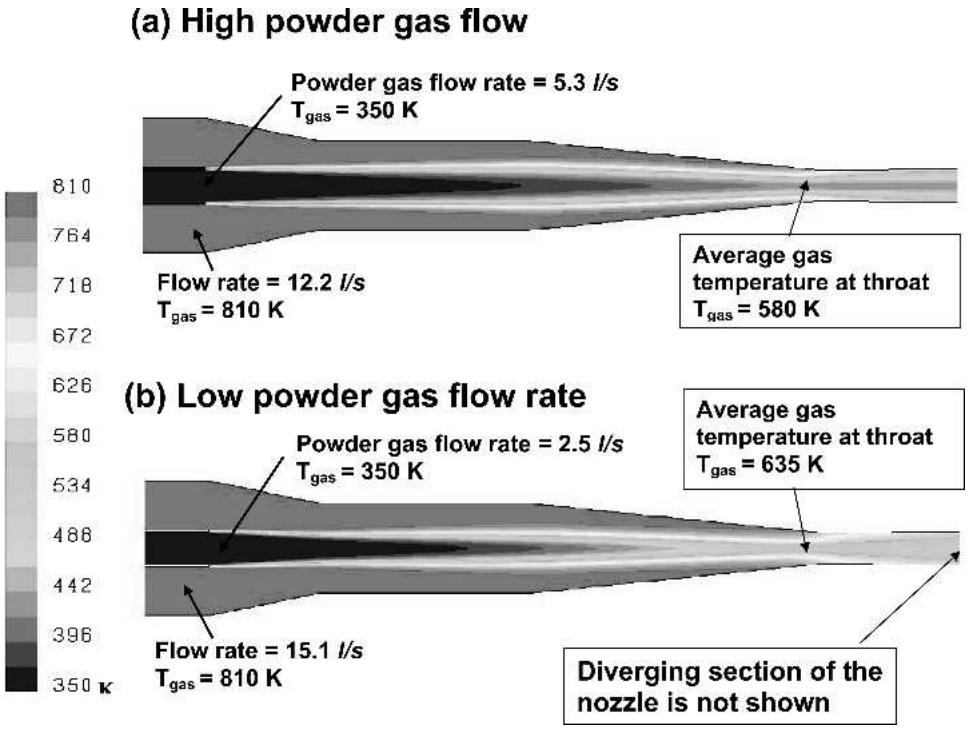

Fig. 15 Effect of powder gas flow rates on the mixture gas temperature at the throat (Diverging section of the nozzle is omitted to emphasize the mixing of the powder gas and the main gas in the pre-chamber and the converging of the nozzle.)

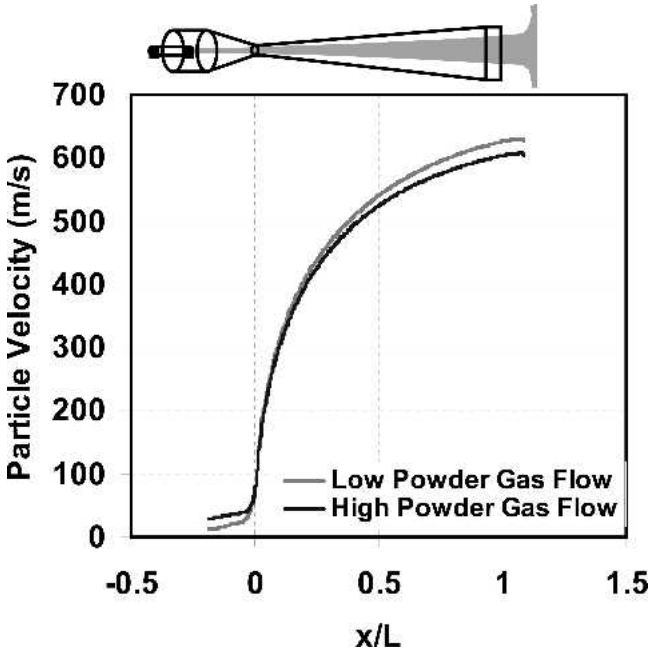

Fig. 16 The computational results showing the aluminum particle velocities for the two cases considered in Fig. 15

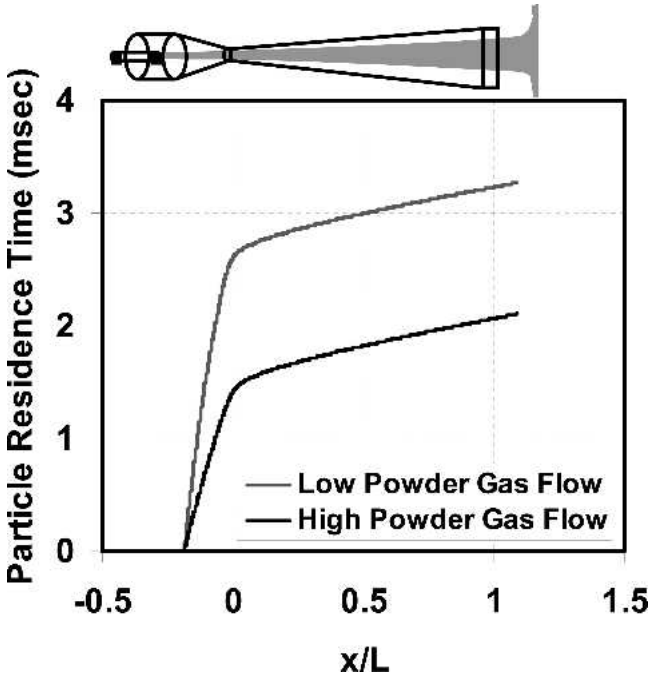

Fig. 17 The computational results showing the aluminum particle residence time for the two cases considered in Fig. 15

throat, as shown in Fig. 16. For the lower powder gas flow rate, the gas velocity surrounding the particles downstream from the powder injector is much smaller as compared with the case of the high powder gas flow rate. Therefore, a relatively large residence time was predicted with the low powder gas flow rate and the most of the particle heating occurred before the diverging section of the nozzle where the surrounding gas temperature is

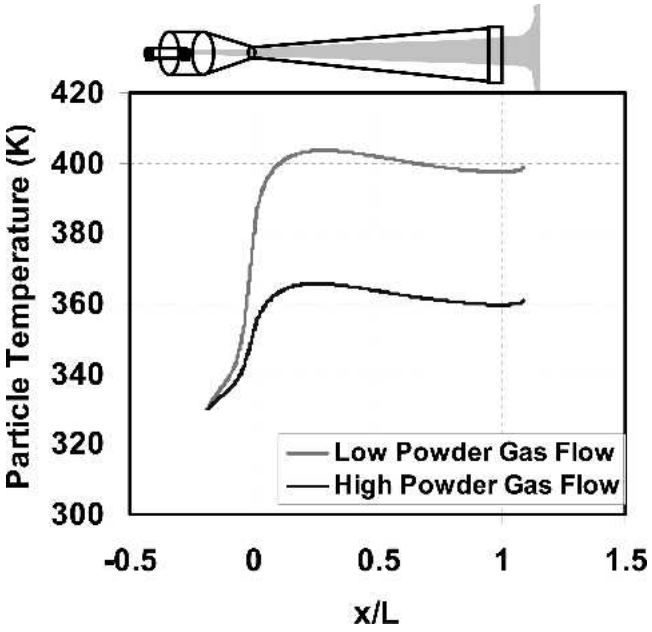

Fig. 18 Computational results showing the aluminum particle temperatures for the two cases considered in Fig. 15

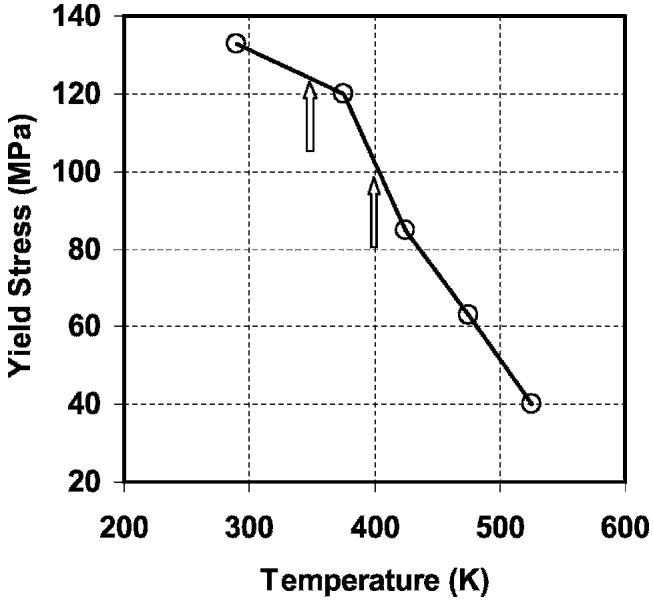

Fig. 19 Effect of material temperature on the yield stress of aluminum (Ref 22)

still relatively high and also due to the relatively large residence time. As shown Fig. 16, the particle velocity for the low powder gas flow rate was predicted to be larger than that for the high powder gas flow rate by ~20 m/s at the exit of the nozzle, even though the particle velocity was smaller in the converging section of the nozzle. This could be a result of the higher average temperature of the mixture gas at the throat for the low powder gas flow rate. Most of the particle heating occurs before the diverging section of the nozzle due to relatively high surrounding gas temperatures and large residence time associated with the low particle velocities. The particles are heated to nearly 400 K at their arrival of the substrate with the lower powder gas flow, compared with 360 K with the higher powder gas flow (see Fig. 18). Though the increase in particle temperature by 40 K may seem to be small, its effect on yield stress can be significant for Al powders (Ref 22). As shown in Fig. 19, the yield stress of Al decreases rapidly from 360 to 400 K. Based on the analysis of simulated results, the enhanced coating deposition by lowering powder gas flow seems to be resulted from the combined effects of increased particle velocity and particle temperature.

5. Summary

Both computational simulations and experimental studies were conducted to examine the effects of spray conditions on the coating formation by the kinetic spray process. The observations can be summarized as follows:

- The bow shock appears to have little effect on deceleration of large size aluminum particles. Accordingly, the deposition efficiency of aluminum shows little variation as a function of standoff distance.
- Wall roughness affects wall friction and the growth of wall boundary layers. The roughness resulting from particle buildup can significantly reduce the particle velocity, thus adversely affecting coating formation by the kinetic spray process. Therefore, selection of spray conditions or use of other means to keep nozzle interior surface clean and smooth is critically important for consistent nozzle performance in coating formation.
- Spray conditions in the kinetic spray process affect the coating formation through primarily their effects on two fundamental variables: particle velocity and particle temperature. In particular, the main gas temperature appears to be the single most important spray variable due to its direct and strong effects on both particle velocity and particle temperature. Other less dominant variables can also be manipulated to further improve coating deposition by the kinetic spray process. These include main gas pressure, nozzle throat size (thus total gas flow), and powder gas flow rate.
- Increasing particle temperature provides an additional means that can effectively enhance coating formation by the kinetic spray process. This can be particularly useful in the case of using compressed nitrogen (instead of helium) to spray large particles where it is often difficult to accelerate large particles above the critical velocity that allows for coating formation.

Acknowledgments

The authors would like to thank our Delphi collegues Mark K. Krage, Richard E. Teets, Tom H. VanSteenkiste, Alaa Elmousi, Dan Gorkiewicz, and Nilesh Patel for their help and useful discussions. We would also like to express our thanks to Dr. Linos Jacovides for supporting this work.

References

1. A.P. Alkhimov, A.N. Papyrin, V.F. Kosarev, N.I. Nesterovich, and M.M. Shushpanov, Gas Dynamics Spraying Method for Applying a Coating, US Patent No. 5 302 414, April 12, 1994

2. R.C. McCune, A.N. Papyrin, J.N. Hall, W.L. Riggs, and P.H. Zachowski, An Exploration of the Cold Gas-Dynamics Spray Method for Several Materials Systems, *Thermal Spray Science and Technology,* C.C. Berndt and S. Sampath, Ed., ASM International, 1995, p 105
3. R.C. McCune, W.T. Donlon, E.L. Cartwright, A.N. Papyrin, E.F. Rybicki, and J.R. Shadley, *Thermal Spray: Practical Solutions for Engineering Problems,* ASM International, 1996
4. R.C. Dykhuizen, M.F. Smith, D.L. Gilmore, R.A. Neiser, X. Jiang, and S. Sampath, Impact of High Velocity Cold Spray Particles, *J. Therm. Spray,* Vol 8, 1999, p 559
5. R.C. Dykhuizen and M.F. Smith, Gas Dynamic Principles of Spray, *J. Therm. Spray,* Vol 7, 1998, p 205
6. T.H. VanSteenkiste, J.R. Smith, R.E. Teets, J.J. Moleski, and D.W. Gorkiewicz, Kinetic Spray Coating Method and Apparatus, US Patent No. 6 139 913, Oct. 31, 2000
7. T.H. VanSteenkiste, J.R. Smith, R.E. Teets, J.J. Moleski, and D.W. Gorkiewicz, Kinetic Spray Coating Apparatus, US Patent No. 6 283 386 B1, Sep. 4, 2001
8. T.H. VanSteenkiste, J.R. Smith, R.E. Teets, J.J. Moleski, D.W. Gorkiewicz, R.P. Tison, D.R. Marantz, K.A. Kowalsky, W.L. Riggs, P.H. Zajchowski, B. Pilsner, R.C. McCune, and K.J. Barnett, Kinetic Spray Coatings, *Surf. Coat. Technol.,* Vol 111, 1999, p 62
9. T.H. Van Steenkiste, J.R. Smith, and R.E. Teets, Aluminum Coatings via Kinetic Spray with Relatively Large Powder Particles, *Surf. Coat. Technol.,* Vol 154, 2002, p 237
10. A.O. Tokarev, Structure of Aluminum Powder Coatings Prepared by Cold Gas Dynamic Spraying, *Met. Sci. Heat Treat.,* Vol 38, 1996, p 136
11. D.L. Gilmore, R.C. Dykhuizen, R.A. Neiser, T.J. Roemer, and M.F. Smith, Particle Velocity and Deposition Efficiency in the Cold Spray Process, *J. Therm. Spray,* Vol 8, 1999, p 576
12. A.H. Shapiro, *The Dynamics and Thermodyanmics of Compressible Fluid Flow,* The Ronald Press Company, New York, 1953
13. C.B. Henderson, Drag Coefficients of Sphers in Continuum and Rarefied Flows, *AIAA J.,* Vol 14 (No. 6), 1976, p 707
14. D.J. Carlson and P.L. Chambre, Particle Drag and Heat Transfer in Rocket Nozzles, *AIAA J.,* Vol 2, 1964, p 1980
15. FLUENT, "FLUENT 6.1 User's Guide," 10 Cavendish Court, Lebanon, NH
16. T. Stoltenhoff, H. Kreye, H.J. Richter, and H. Assadi, Optimization of the Cold Spray Process, *Thermal Spray: New Surfaces for New Manufacturing,* ASM International, 2001
17. B.E. Launder and D.B. Spalding, The Numerical Computation of Turbulent Flows, *Computer Methods in Applied Mechanics and Engineering,* Vol 3, 1974, p 269
18. R. J. Litchford, and S.M. Jeng, Efficient Statistical Transport Model for Turbulent Particle Dispersion in Sprays, *AIAA J.,* Vol 29, 1991, p 1443
19. V.F. Kosarev, S.V. Klinkov, A.P. Alkhimov, and A.N. Papyrin, On Some Aspects of Gas Dynamics of the Cold Spray Process, *J. Therm. Spray,* Vol 12, 2003, p 265
20. L.F. Moody, *ASME Trans.,* Vol 66, 1944, p 671
21. T. Cebeci and P. Bradshaw, *Momentum Transfer in Boundary Layers,* Hemisphere Publishing Corporation, 1977
22. A. Buch, *Pure Metals Properties: A Scientific-Technical Handbook,* ASM International, Materials Park, OH, and Freund Publishing House Ltd., 1999, p 242